Electromechanical Energy Conversion Systems (EECS)
Niroo Research Institute (NRI)
Vol. 4, No. 1, Spring 2025, pp. 30- 35
DOI: 10.30503/EECS.2024.483451.1063
Original Article

Design of Permanent Magnet Synchronous Motor (PMSM) for Use in Electric Vehicles (EVs)

Vahid Zamani Faradonbeh [1,2*], Mohammad Alaei Faradonbeh [1,3], Amir Rashidi[4]

Abstract

In this paper, the consequent pole-type brushless Permanent Magnet Synchronous Motor (PMSM) is designed for an Electric Vehicle (EV) with a gross weight of 1800 kg. The EV can travel on a road with a maximum slope of 20% with a maximum speed of 100 km/h and on a road without a slope with a maximum speed of 150 km/h. Due to the use of the consequent method, the cost of magnets has been reduced. The PMSM motor is an Interior Permanent Magnet (IPM) type with a single-layer U-shaped PM. Results such as distribution of flux density, torque, core, and ohmic losses have been obtained. The torque-speed and power-speed curves are important diagrams of EV motor analysis that will be obtained. The results of the efficiency map show that the motor efficiency is mostly above 96%. The results and curves of PMSM performance are simulated using Maxwell software.

Keywords: Permanent Magnet Synchronous Motor (PMSM), Electric Vehicle (EV), Consequent Pole.

Received Date:2024-10-14; Revised Date: 2024-11-28; Accepted Date:2025-05-03

1. INTRODUCTION

Permanent magnet synchronous motors offer several benefits compared to induction machines, including greater torque density, simplified control techniques, improved power factor, and enhanced efficiency. PMSMs can be classified based on their permanent magnet configurations into four categories: Surface-Mounted Permanent Magnet (SPM), Surface Inset Permanent Magnet (SIPM), Interior Permanent Magnet, and Spoke Interior Permanent Magnet (Spoke IPM). Each of these configurations presents unique advantages and drawbacks. A comparative analysis of these structures is presented in Table 1 [1].

The use of IPMs has become common across various industrial sectors, because of impressive benefits. These include high power density, a broad constant-power speed range, excellent mechanical robustness, and outstanding efficiency. As a result, when evaluated against induction machines and SPM/SIPM, IPMs stand out as suitable alternatives in many performance-sensitive applications. These machines are particularly favored in Electric Vehicle (EV) applications due to their excellent features, such as high power density, a wide constant-power speed range, and strong resistance to mechanical stress [2]-[4].

TABLE. 1. Comparison between the structures of PMSM [1]

	SPM	SIPM	IPM	Spoke IPM
Cost	Low	Low	High	Medium
Robustness	Low	Medium	Very high	High
Maximum speed	Low	Medium	High	High
D/Q axis reluctance		>1	>1	<1
Magnet Eddy current losses	High	Medium	Low	Low
Harmonics in PM due to stator MMF	High	Medium	Low	Low
Power extension capability	Low	High	Very high	Very high

The configurations of their rotor topologies greatly influence the performance of Interior Permanent Magnet machines. A common rotor design utilized in

[1] *Faraz Tavan Electric Machines Company, Iran*
[2] *Electrical Engineering Department, Shiraz University of Technology, Shiraz, Iran*
[3] Department of *Electrical and Computer Engineering, Isfahan University of Technology, Isfahan, Iran*
[4] Department of *Electrical and Computer Engineering, Hakim Sabzevari University, Sabzevar, Iran*

electric vehicle applications is the V-shape IPM machine, exemplified by models such as the 2004 Toyota Prius, the 2007 Camry, and the 2010 Prius. Numerous V-type rotor configurations have been documented in the literature concerning electric vehicle applications. Comparisons have been conducted between the V-shape IPM machine, induction motor (IM), and switched reluctance motor (SRM), focusing specifically on their application in electric vehicles (EV) and hybrid electric vehicles (HEV) [6]. The findings demonstrate that the V-shape IPM machine exhibits superior power density and efficiency compared to both the IM and SRM. A comparison is also drawn between the V-shape IPM machine and the surface-mounted PM machine regarding their use in hybrid traction applications. The findings from [7] suggest that the V-shape IPM machine demonstrates a wider constant power speed range and lower PM eddy current losses in comparison to the surface-mounted PM machine. Furthermore, the spoke shape, tangential shape, U-shape, and V-shape IPM machines have been designed and assessed for their applicability for use in electric vehicle applications [8]. The results indicate that the V-type IPM machine shows enhanced average torque and power factor, as well as diminished torque ripple in comparison to the other configurations. The study encompasses an analysis of the V-type, tangential type, U-type, and 2U-type in the context of traction applications [9]. Also, the findings in [9] indicate that the V-type IPM machine exhibits superior power, torque, and rotor saliency. A comparison between the V-type and V+U type configurations reveals that the V+U type rotor is more helpful in minimizing harmonic losses due to the eddy current in the stator teeth than the V-type rotor, as evidenced by the results presented in reference [10]. Additionally, the ∇-shape rotor is identified as another conventional topology suitable for electric vehicle applications, e.g., the Lexus LS600H [5]. The ∇-type IPM machine has been enhanced to minimize core loss, as indicated in [11]. The findings demonstrate a significant reduction in iron loss, despite a minor reduction in average torque. Additionally, the V-type, 2V-type, and ∇-type IPM machines have been evaluated for applications requiring elevated torque density [12], the results suggest that the ∇-type machine is among the most effective designs for minimizing cross-magnetization effects in high torque density applications. A model of the 2V-shape machine has been introduced to forecast the actual performance of the machine [13], and the outcomes demonstrate that this model is both computationally effective and numerically dependable. Additionally, a 2U-type motor featuring an artificial flux linkage model has been suggested for use in EV applications [14]. The U-shape is used in this paper. The U-shape structure has a good flux linkage, which increases the torque density. Consequent-pole (CP) motors can operate at the same torque level as PM motors without CP but at a lower PM volume [15]. Also, CP motors can operate at a higher efficiency compared to PM motors without CP motors [15].

This study presents the design of an electric vehicle motor, intended for a total weight of 1800 kg and a top speed of 150 km/h, utilizing Ansys Maxwell software. Also, the maximum slope of the road for the car is 20%. The consequent method has been used to reduce the cost of magnets in the IPM structure.

2. DESIGN AN ELECTRIC MOTOR FOR EV

According to the contents stated in the introduction, the PMSM motor is recommended as an EV motor. Among the common structures of the PMSM motor (SPM, SIPM, and IPM), the IPM structure is suggested due to the advantages mentioned. The structure of IPM has different topologies, such as V-shape, U-shape, spoke-shape, etc. Also, this structure can be multi-layered. This study employs a consequential structure in an IPM motor featuring U-shaped permanent magnets, which effectively lowers the cost of the magnet.

To calculate the power and torque of the electric motor, the car's specifications are needed. The specifications of the EV are given in Table 2.

TABLE2.Vehicle characteristics

Net Weight (Kg)	1500
Gross Weight (Kg)	1800
Inclination angle (a), deg	11.3
EV cross-sectional area (m^2)	2.03
Drag coefficient (Cw)	0.363
Max Speed (Km/h)	150
Tire radius (m)	Almost 0.28
Tire diameter	56 cm

The gross weight and net weight are EV's weight with and without the passenger's weight, respectively. For electric car applications, we also need to know the PCD & CB of matched wheelrim. PCD and CB are 100mm and 54mm, respectively.

The torques applied to the car on the road with a maximum slope of 20% and the road without slope are as follows:

$$F_c = M\ g\ \sin(\mathrm{a}) \tag{1}$$

$$F_r = C_r\ M\ g\ \cos(a) \tag{2}$$

$$F_w = 0.5\ \rho_{air}\ S\ C W\ V_s{}^2 \tag{3}$$

$$T_s = (\mathrm{F}_c + \mathrm{F}_r + \mathrm{F}_w)\,\mathrm{R}_{out}\big|_{a=11.3\deg \,\&\, V_s=20.5\,m/s} \quad (4)$$

$$T_s' = (\mathrm{F}_c + \mathrm{F}_r + \mathrm{F}_w)\,\mathrm{R}_{out}\big|_{a=0\deg \,\&\, V_s=41.6\,\mathrm{m/sec}} \quad (5)$$

The Ts and Ts' obtained 1120 and 320 N.m, respectively, where Fc, Fr, and Fw, are climbing resistance, rolling resistance, and wind age resistance, respectively. Ts is the required torque in the road with and without slope. M is the total weight of the car and passengers (1800kg). g is the acceleration of gravity (9.81 m/s^2). Cr represents the coefficient of rolling resistance and is equal to 0.0188 for car tires on tar or asphalt. ρ_{air} S, CW, and Vs are air density, frontal area of the vehicle, coefficient characterizing the body shape and aerodynamic quality of the vehicle (drag coefficient), and vehicle speed, respectively. The torque values obtained in (4) are for the wheel of the vehicle. When the car moves on the road with a 20% slope, its top speed is 100 km/h, and the torque on the wheel is 1120 Nm. When the car moves on the road without a slope, the top speed of the car is 150 km/h, and the required wheel torque is 320 Nm. If we consider the gear conversion ratio of 10 and the efficiency of 80%. The motor's rated torque is 140 N-m, rated power is 106 kW, rated speed is 7000 rpm, and top speed is 14200 rpm.

The electrical characteristics of the designed motor are given in Table 3. The IPM is designed with U-shaped magnets. Consequent IPM (CIPM) method is used for this Motor. Using the CIPM structure reduces the volume of the magnet (reduces the cost), increases the mechanical strength of the motor, and minimizes the eddy current losses associated with the magnet. This method produces more ripple torque, which we have reduced by using ripple reduction methods.

The motor output power is directly related to motor size and speed (6).

$$P_{out} = C_0\, B_{ag}\, ac\, D_{ag}^2\, L_{stk}\, \omega \quad (6\text{-a})$$

$$C_0 = \frac{4.44\,\pi\, k_w}{8} = 1.57 \quad (6\text{-b})$$

Where Parameters L_{stk} and Dag represent the active axial length and the air-gap diameter, respectively. The B_{ag} is the air-gap flux density and is obtained via the magnetic circuit (MC) model, ac is the electrical loading, C_0 is a constant parameter, and k_W is the winding factor.

B_{ag} and ac are calculated via the MC model and compared to their initial values. If the difference is significant, the algorithm goes through a repetitive process until they converge.

$$D_{ag}^2\, L_{stk} = \frac{P_{out}}{C_0\, B_{ag}\, ac\, \omega} \quad (7)$$

The flux density within the airgap is determined using the magnetic circuit (MC) model (3-a), which closely approximates the initial or assumed value.

$$B_g^{\max} = \frac{B_{rem}^I h_{m1}}{h_a + \frac{l_g h_{m1}}{l_m}} - \frac{N_m B_{sat} h_{sat}}{h_a} \quad (8)$$

where B_{rem}^I is the PM remanent flux density for IPMSMs. The lg and l_m are the air-gap length and permanent magnet thickness, respectively. Nm is the number of bridges per pole, B_{sat} is the saturation of the rotor bridge flux density, h_{sat} is the bridge thickness, and hm1 and ha are, respectively, the PM average length and average circumferential length in the air gap per pole.

The maximum flux density in the airgap (ϕ_{max}) and the winding turn number per phase (N_t) are calculated by (9).

$$\phi_{\max} = \frac{B_{ag}\, L_{stk} D_{ag}\, \pi}{2p} \quad (9\text{-a})$$

$$N_t = \frac{V_{ph}}{4.44\, f\, \phi_{\max}\, k_{ws}} \quad (9\text{-b})$$

where V_{ph} is the effective value of the phase voltage. The p is pole pairs. The electrical loading is calculated via (10).

$$Q_{in} = \frac{P_{out}}{\eta\, PF} \quad (10\text{-a})$$

$$I_{ph} = \frac{Q_{in}}{3 \times V_{ph}} = \frac{61.1}{3 \times \frac{12}{\sqrt{3}\sqrt{2}}} = 4.157\ amper \quad (10\text{-b})$$

$$ac = \frac{2mN_t I_{ph}}{D_{ag}\,\pi} = \frac{2 \times 3 \times 27 \times 4.157}{0.0242\pi} = 8850 \quad (10\text{-c})$$

The maximum power and maximum torque are obtained by Newton's second law (11). According to Newton's law, the EV travels from 0 to 100 km/h in 6.3 sec. Where T_{max} is the maximum torque of the motor, it is equal to 300 Nm (twice the rated torque).

$$F_{ac} = M\ a_c = M\ \frac{\Delta V_s}{\Delta t} \quad (11\text{-a})$$

$$\Delta t = \left. \frac{M \ \Delta V_s}{\frac{T_{\max}}{R_{out}}} \right|_{speed\ from\ 0-100 km/h} \quad (11\text{-b})$$

TABLE 3: Specifications of the motor

Rotor type	CIPM-U
Cooling type	Indirect liquid
Number of poles	10
Number of Slots	30
Stator OD	190 mm
Stator stack length	225 mm
Motor stack length	370 mm
Stator/Rotor mass	28 / 15 kg
Air gap length	1 mm
PM volume	281 cm^3
Copper mass	4.5 Kg

3. RESULTS

The two-dimensional (2-D) and three-dimensional (3-D) structure of the rotor and stator of the CIPM motor is shown in Fig. 1.

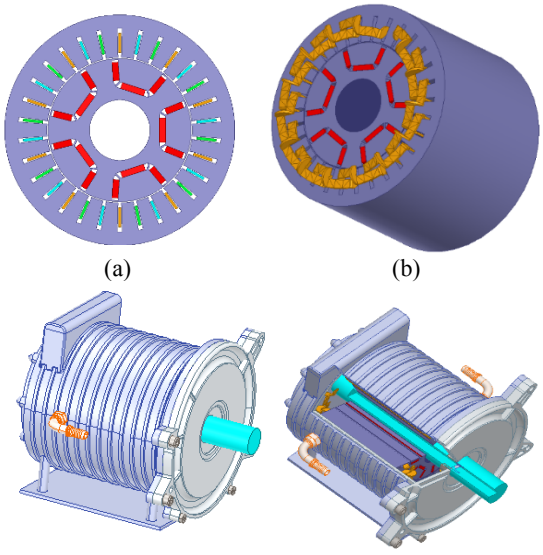

(a) (b) (c)

Fig. 1. a) 2-D. b) 3-D structure of the rotor/ stator, and c) full body of CIPM.

The material of the stator and rotor sheet is 1008 steel. The saturation limit for steel is 1.9 Tesla. Fig. 2 shows the flux density distribution at the rated power. Considering that the flux lines tend to pass through the path with lower reluctance, the motor bridges will always go into saturation. The maximum tooth flux density is 1.7 Tesla, and the maximum stator yoke flux is 1.6 Tesla. The motor wiring pattern is shown in Fig. 2.

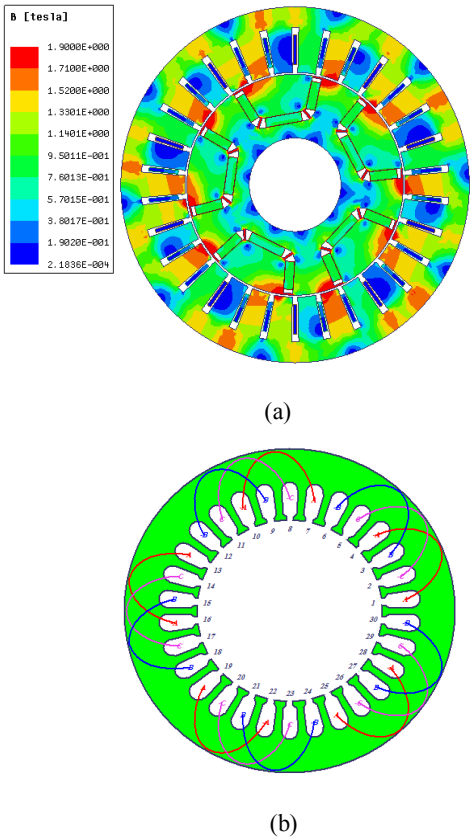

(a) (b)

Fig. 2. a) The flux density distribution at rated power and b) wiring pattern.

In this part, the motor is injected by a three-phase sinusoidal current with a frequency of 585 Hz, and the motor operates at a constant speed of 7020 revolutions per minute. In order to achieve an average torque of 150 N-m, the peak current must be 390 amperes. Fig. 3 illustrates the motor torque curve. The mean torque measures 152 N-m, with a torque ripple amplitude of 12 Nm. Consequently, the output power is estimated to be around 111 kW.

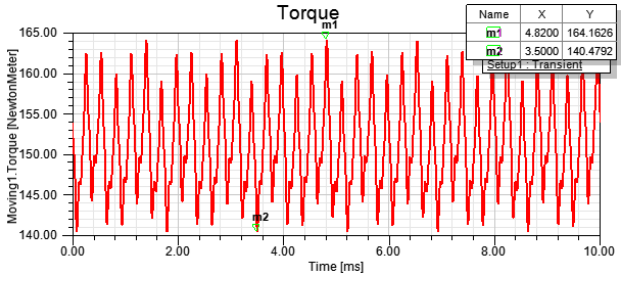

Fig. 3. Electrical Torque.

The core and copper losses are 1.35 and 1.65 kilowatts, respectively. Mechanical losses of the motor (friction of bearings, etc.) are presumed to pertain to 1% of output power, so the efficiency is 96.3%.

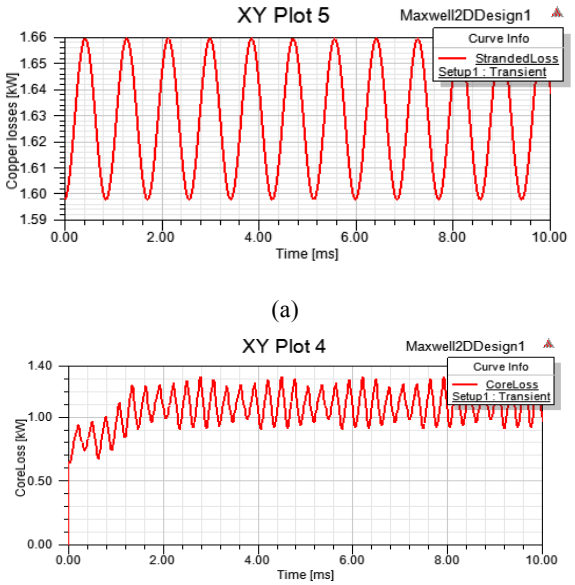

Fig. 4. a) The core and b) copper losses.

The motor is required to meet five operational points illustrated in Fig. 6, which depicts the target torque and power curves relative to the rotational speed. The operating point 1 (155 Nm & 0 rpm) indicates the maximum torque that can be delivered at the rim at the initial stage. The torque value is calculated based on the overall load of the vehicle when ascending a gradient of 20%. Working point 2 (152 Nm & 7000 rpm) indicates the rated torque and rated power. In working points 3 and 4 (7000<speed<14200), the motor is in flux-weakening operation. When the car's speed is more than 100 km/h, the motor enters this area. The operational point of 14200 rpm signifies the maximum speed. At speeds exceeding 14200 rpm, the vehicle operates in high-speed thermal mode to produce energy for battery charging.

The curves of cogging torque and back-EMF of the line in no-load operation for the motor are given in the figure below. The Maximum cogging torque value is 4 N-m.

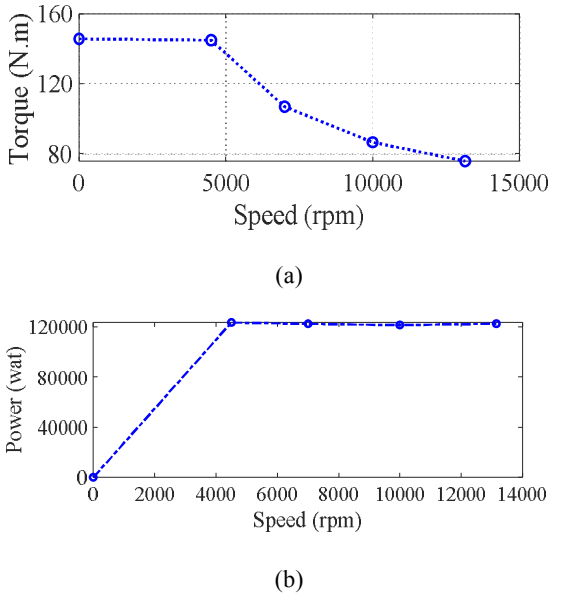

Fig. 5. a) The torque and b) the power specifications.

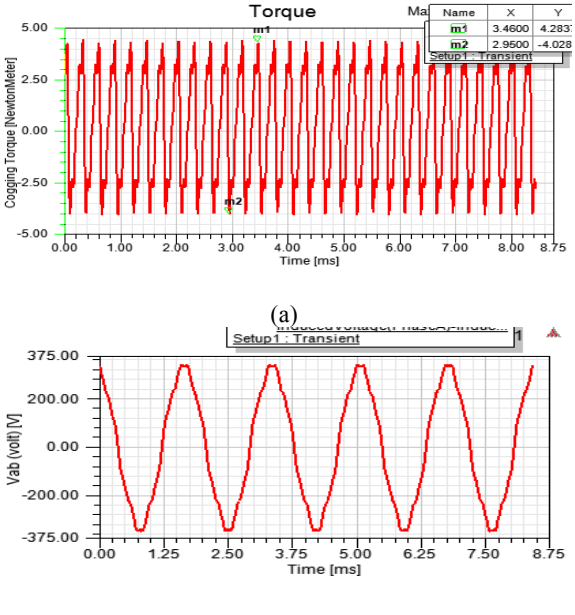

Fig. 6. a) The cogging torque and b) Back-emf.

Finally, the motor efficiency map is presented in Fig. 7.

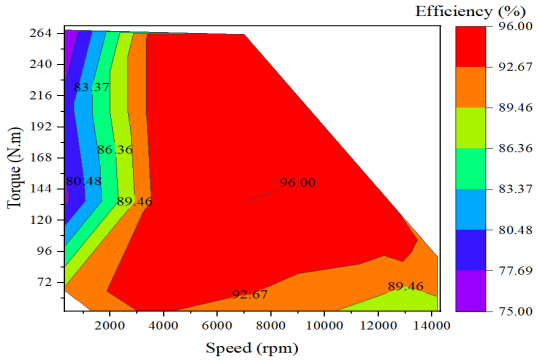

Fig. 7. The efficiency map.

The CP motor performance results are reported in Table 4.

TABLE 4: The result of the designed motor.

Rate Power		110 kW
Rate Torque		150 N-m
DC Link Voltage		380 volts
Rate Speed		7000 rpm
Maximum speed		14200 rpm
Max Power		220 kW
Peak of Phase Current		390 A
Efficiency		96.3%
Average torque to torque ripple (TR)		12.66
Power losses	Copper	1.65 kW
	Core	1.35 kW
	Mech	1.1 kW

4. CONCLUSIONS

In this work, an IPM motor with U-shaped PMs was designed for use in EVs. The consequent pole type was used to reduce the PM by 50%. According to the efficiency map, the motor efficiency is mostly 96%. This motor can move an EV weighing 1800 kg on a non-sloping road at a top speed of 150 km/h. Also, the results show that the car can move on the road with a maximum slope of 20%.

REFERENCES

[1] A. Rahideh, M. Mardaneh and T. Korakianitis, "Analytical 2-D Calculations of Torque, Inductance, and Back-EMF for Brushless Slotless Machines With Surface Inset Magnets," in *IEEE Transactions on Magnetics*, vol. 49, no. 8, pp. 4873-4884, Aug. 2013, doi: 10.1109/TMAG.2013.2242087.

[2] V. Z. Faradonbeh, A. Rahideh, S. T. Boroujeni, "2-D Analytical No-Load Electromagnetic Model for Slotted Interior Permanent Magnet Synchronous Machines," IEEE Trans. Energy conv, vol. 36, no. 4, pp.3118-3126, Dec. 2021.

[3] V. Z. Faradonbeh, E. Amiri, "Open-Circuit Electromagnetic Analysis of Interior Permanent Magnet Machines with Arbitrary Rotor Frame Using a 2-D Analytical Model," *IEEE Trans. Magn*, vol. 58, no. 8, Aug. 2022..

[4] M. M. Ghahfarokhi, V. Z. Faradonbeh, E. Amiri and etc "Computationally Efficient Analytical Model of Interior Permanent Magnet Machines Considering Stator Slotting Effects," *IEEE Trans. Industry Applications*, vol. 58, no. 4, July-Aug. 2022.

[5] M. Olszewski, "Evaluation of the 2010 Toyota Prius hybrid synergy drive system," *Oak Ridge Nat. Lab*., U.S. Dept. Energy, 2011.

[6] Zhi Yang, Fei Shang, IanP. Brown, and Mahesh Krishnamurthy, "Comparative Study of Interior Permanent Magnet, Induction, and Switched Reluctance Motor Drives for EV and HEV Applications," *IEEE Trans. Transp. Electrif.*, vol. 1, no. 3, pp. 245-254, Oct. 2015.

[7] Patel B. Reddy, Ayman M. El-Refaie, Kum-Kang Huh, Jagadeesh K. Tangudu, and Thomas M. Jahns, "Comparison of Interior and Surface PM Machines Equipped With Fractional-Slot Concentrated Windings for Hybrid Traction Applications," *IEEE Trans. Energy Convers*., vol. 27, no. 3, pp. 593-602, Sep. 2012.

[8] Xiangdong Liu, Hao Chen, Jing Zhao, and Anouar Belahcen, "Research on the Performances and Parameters of Interior PMSM Used for Electric Vehicles," *IEEE Trans. Ind. Electron.*, vol. 63, no. 6, pp. 3533-3545, Jun. 2016.

[9] Katteden Kamiev, Juho Montonen, Mahendarkar Prabhakaran Ragavendra, Juha Pyrhönen, JuanA.Tapia, and Markku Niemelä, "Design Principles of Permanent Magnet Synchronous Machines for Parallel Hybrid or Traction Applications," *IEEE Trans. Ind. Electron.*, vol. 60, no. 11, pp. 4881-4890, Nov. 2013.

[10] Seok-Hee Han, Wen L. Soong, Thomas M. Jahns, Mustafa K. Guven, and Mahesh S. Illindala, "Reducing Harmonic Eddy-Current Losses in the Stator Teeth of Interior Permanent Magnet Synchronous Machines During Flux Weakening," *IEEE Trans. Energy Convers*., vol. 25, no. 2, pp. 441-449, Jun. 2010.

[11] Katsumi Yamazaki, Masaki Kumagai, Takeshi Ikemi, and Shunji Ohki "A Novel Rotor Design of Interior Permanent-Magnet Synchronous Motors to Cope with Both Maximum Torque and Iron-Loss Reduction," *IEEE Trans. Ind. Appl.*, vol. 49, no. 6, pp. 2478-2486, Nov/Dec. 2013.

[12] Katsumi Yamazaki, and Masaki Kumagai, "Torque Analysis of Interior Permanent-Magnet Synchronous Motors by Considering Cross-Magnetization: Variation in Torque Components with Permanent-Magnet Configurations," *IEEE Trans. Ind. Electron*., vol. 61, no. 7, pp. 3192-3201, Jul. 2014.

[13] Xiao Chen, Jiabin Wang, Bhaskar Sen, Panagiotis Lazari, and Tianfu Sun, "A High-Fidelity and Computationally Efficient Model for Interior Permanent-Magnet Machines Considering the Magnetic Saturation, Spatial Harmonics, and Iron Loss Effect," *IEEE Trans. Ind. Electron.*, vol. 62, no. 7, pp. 4044-4055, Jul. 2015.

[14] Seungho Lee, Yu-Seok Jeong, Yong-Jae Kim, and Sang-Yong Jung, "Novel Analysis and Design Methodology of Interior Permanent-Magnet Synchronous Motor Using Newly Adopted Synthetic Flux Linkage," *IEEE Trans. Ind. Electron.*, vol. 58, no. 9, pp. 3806-3814, Sep. 2011

[15] J. Li, K. Wang, and C. Liu, "Torque improvement and cost reduction of permanent magnet machines with dovetailed consequent-pole rotor," *IEEE Trans. Energy Convers.*, vol. 33, no. 4, pp. 1628-1640, Dec. 2018.